Multiple radio transmitter localization via UAV-based mapping

Multiple Radio Transmitter Localization via UAV-based Mapping

Zhuyin Li, *Student Member, IEEE,* Andrea Giorgetti, *Senior Member, IEEE,* and Sithamparanathan Kandeepan, *Senior Member, IEEE*

***Abstract*—The widespread use of unmanned aerial vehicles (UAVs) has opened a novel perspective on spectrum awareness and localization because of their ability to overcome spatial limits and the burden of dedicated infrastructure. In such scenarios, an underinvestigated problem is the simultaneous localization of multiple non-collaborative primary users (PUs) of the spectrum, whose number, transmit power, activity pattern, and signal structure are unknown. This work proposes a framework for multiple PU localization based on the received power measured by an antenna array mounted on a UAV. A score map is firstly constructed based on the measured power. Then two algorithms, k-means clustering and weighted centroid (KCWC), and Gaussian mixture model fitting (GMMF) are applied to the score map to estimate the number and the positions of the PUs. The performance is evaluated in terms of optimal subpattern assignment (OSPA) distance, compared with a genie-aided (GA) localization algorithm capable of separating the signals emitted by the PUs. Despite the blind nature of the method proposed, numerical results exhibit very good localization accuracy, with an OSPA distance below 6 m in large, line-of-sight (LOS)-dominated, outdoor scenarios with five PUs, even in the presence of channel impairments and UAV position and heading uncertainties.**

***Index Terms*—Multiple targets, non-collaborative localization, antenna array, clustering, Gaussian mixture model, unmanned aerial vehicle.**

I. Introduction

SPECTRUM awareness in space and the geolocation of radio transmitters are essential aspects for a wide range of technologies, including Internet-of-Things (IoT), cyber-physical systems, wireless sensor networks (WSNs), and dynamic spectrum sharing/access in cognitive radio (CR) systems [1]–[3]. The knowledge of spectrum occupancy and how it is utilized by devices in space-time are shifting focus in the research domain from spectrum sensing [4] to the more sophisticated spectrum utilization prediction [5] and wireless networks topology inference [6]. However, such augmented knowledge requires geolocation of the spectrum users as a driving technique [7]–[9]. With the development of unmanned aerial vehicles (UAVs), the existing ground-based wireless communication networks can be extended up to air-to-ground (A2G) communication networks, offering unique advantages such as short-range line-of-sight (LOS) dominated paths, high mobility, less influence from terrestrial constraints, and fast deployment and configuration [10]–[12]. Likewise, spectrum awareness and geolocation may benefit the assistance of UAVs to have mobile agents/anchors, thus overcoming geographical limits and the burden of dedicated infrastructure. However, such an interesting scenario comes along with numerous challenges: design effective algorithms, take advantage of LOS paths, plan UAVs trajectories and positions, understand the impact of A2G channel, face the lack of collaboration with the target in some scenarios or the lack of knowledge about the target signaling (modulation type, packet format), to name a few.

In the conventional ground-based scenarios, i.e., CR networks, when very limited information about the primary users (PUs) is available, weighted centroid localization (WCL) has been widely proposed as an attractive low-complexity solution [13]–[16]; and its performance has been evaluated considering different aspects of propagation [17]–[19]. To improve the localization accuracy of WCL, the ambiguous anchor nodes are removed by comparing the closeness and evenness to the target in [20]. In [21], a mean-shift-based algorithm clusters the nodes based on their distance to the target iteratively to achieve a flexible node selection on a large scale WSN. In [16], the WCL principle has been extended in the cyclic frequency domain by using the cyclic autocorrelation of the received signals as weights to robustify WCL under the presence of interference or simultaneous transmissions.

On the other hand, more sophisticated solutions are based on maximum likelihood (ML) [22], support vector regression [23], and a joint regression and clustering method [24]. Beyond received signal strength (RSS)-only-based localization techniques, hybrid techniques can achieve a more accurate estimate of the target. For example, [25] localizes the radio source by a score map built from measured RSS and coarse direction-of-arrival (DoA) with sectorial antennas equipped by the receiver nodes. A dual problem is addressed in [26], where transmitters equipped with sectorial antennas perform a sector fitting localization method based on the geolocation and the cell ID of the sensors. Another hybrid method which combines RSS and time-of-arrival (ToA), proposed in [27], [28], uses two signature vectors, extracted by the tensor decomposition, to localize the target.

All the above works consider a single target in the monitored

This work was supported by MIUR under the program "Departments of Excellence (2018-2022) - Precise-CPS," and the CoACh project funded by the POR FESR 2014-2020 program. Part of this work will be presented at the European Signal Proc. Conf. (Eusipco 2020), Amsterdam, Jan. 2021.

Z. Li and S. Kandeepan are with the School of Engineering, RMIT University, Melbourne VIC 3001, Australia (e-mail: s3666118@student.rmit.edu.au, kandeepan.sithamparanathan@rmit.edu.au).

A. Giorgetti is with the Department of Electrical, Electronic, and Information Engineering "Guglielmo Marconi," CNIT, University of Bologna, Cesena 47522, Italy (e-mail: andrea.giorgetti@unibo.it).

area, an assumption seldom true. Multiple targets bring more challenges to the localization problem. For a general multiple target localization task, two fundamental questions should be answered: i) how many targets are in the area? ii) what are their positions? Single-source localization algorithms can be adopted to solve the problem if the transmissions can be distinguished and separated, e.g., by a unique ID or because their physical layer specifications are known. Unfortunately, especially in the CR context, with limited knowledge of the primary network, the radio sources can hardly be distinguished from the received radio signals. For example, in [29] the city map is used to optimize the UAV trajectory and to simplify the localization. The work shows that if the number of PUs is known, the multiple user localization can be decomposed into several single-user localization problems solved via standard least square (LS) by segmenting the LOS and non-line-of-sight (NLOS) paths. However, it might be challenging to obtain information on the environment and the number of users in a CR context. Some relevant works solving both questions above include [2] that proposes a soft-information (SI)-based localization technique that depends on the likelihood functions of the signal features as well as the propagation context. Compared with the conventional single-value-based (angle/range metrics) hard localization techniques, the SI-based technique achieves a more accurate performance by considering richer information from both inter- and intra-nodes but with a substantial increase in complexity. From a different perspective, [30] and [31] present non-parametric algorithms based on the energy measurements, with no prerequisite on the propagation model. Such algorithms intelligently take advantage of the symmetry and unimodality features of the propagation of single or multiple sources; however, their performance degrades with the source number.

To tackle the existing gaps in the radio localization of non-collaborative multiple targets, we propose two novel algorithms, which provide solutions for both the fundamental goals, namely the detection of target number and the estimation of their position. To summarize, our main contributions are:

1) We propose a UAV-assisted multiple radio source localization framework that takes advantage of the A2G communication, for example, minimizing the infrastructure;
2) We propose two localization algorithms, k-means clustering and weighted centroid (KCWC) and Gaussian mixture model fitting (GMMF), to estimate the number and the positions of multiple non-collaborative transmitters. The proposed algorithms rely on simple RSS measured by a steering antenna array onboard the UAV. The methodology developed is blind, allowing localization of multiple transmitters whose key features (i.e., number, modulation type, physical layer signaling) are unknown.
3) We propose to evaluate the localization performance in terms of optimal subpattern assignment (OSPA) distance [32], which measures the accuracy of estimation of the number of PU and the accuracy of their position estimates in one single metric. Numerical results show that the proposed algorithms can achieve $3-7$ m localization accuracy also in the presence of measurement uncertainties and random PUs topology. Such results are satisfying when compared with a genie-aided (GA) method, wherein transmitted signals are perfectly separated and thus localized individually.

Throughout the paper, capital boldface letters denote matrices, lowercase bold letters denote vectors, $(\cdot)^{\mathrm{T}}$ stands for transposition, $\det(\cdot)$ stands for the determinant of a matrix, and $||\cdot||_p$ is the l_p-norm.

The remainder of the paper is organized as follows. In Section II, the general system model of the problem is presented. The proposed algorithm is discussed in Section III and Section IV. A case study is illustrated in Section V, followed by the performance evaluation in Section VI. Conclusions are drawn in Section VII.

II. System Model

We address the non-collaborative localization of simultaneously transmitting PUs exploiting a single UAV. Let us consider N PUs, operating at carrier frequency f_{C}, at locations, $\boldsymbol{\ell}_{\mathsf{P}}^n = [x_{\mathsf{P}}^n, y_{\mathsf{P}}^n, z_{\mathsf{P}}^n]$, $n = 1, \ldots, N$, in a square area of side length $\mathscr{L}$, as depicted in Fig. 1. The number of PUs, N, their transmit power, P_{T}^n, $n = 1, \ldots, N$, as well as their positions, $\boldsymbol{\ell}_{\mathsf{P}}^n$, $n = 1, \ldots, N$, are unknown.

The UAV cruises over the area, listening to the signals transmitted by the PUs and taking M measurements along its pre-planned trajectory, at the height z_{UAV}, to perform localization. The UAV is equipped with a positioning system, a RSS sensor and a uniform linear array (ULA) with beam steering capabilities. Therefore, each measurement data set, $\boldsymbol{\mathcal{m}}^m$, includes three pieces of information, $\boldsymbol{\mathcal{m}}^m = \{\boldsymbol{\ell}^m, \eta^m, \mathbf{p}^m\}$, $m = 1, \ldots, M$, where $\boldsymbol{\ell}^m = [x^m, y^m, z_{\mathsf{UAV}}]$ is the UAV location and η^m its heading direction angle, both provided by the positioning system, while $\mathbf{p}^m$ is a vector keeping track of the RSSs per steering direction. The definition and construction of $\mathbf{p}^m$ will be given later in this section.

The ULA is electronically steered step-by-step with a step size equal to the beamwidth, Δ_ϑ, to cover 2π. As a result, the rotation generates $S = 2\pi/\Delta_\vartheta$ steering directions, with the sth direction $\vartheta_s^m = \vartheta_1^m + \Delta_\vartheta(s-1)$, $s = 1, \ldots, S$. For each measurement, the first steering direction is always aligned with the heading direction of the UAV, i.e., $\vartheta_1^m = \eta^m$. Without loss of generality, we consider a ULA composed of U isotropic elements, whose array factor (AF) is given by [33]

$$\mathsf{AF}(\varphi) = \frac{\sin\left(\hbar U \frac{\Delta_{\mathsf{U}}}{2}\sin(\varphi)\right)}{\sin\left(\hbar \frac{\Delta_{\mathsf{U}}}{2}\sin(\varphi)\right)} \tag{1}$$

where $\hbar = 2\pi f_{\mathsf{C}}/v_{\mathsf{C}}$ is the wave number, with v_{C} the speed of light, Δ_{U} is the inter-element spacing, and $\varphi \in [-\pi/2, \pi/2]$ is the broadside angle, with $\varphi = 0$ indicating a direction orthogonal to the array axis. The ULA gain is related to the AF by

$$G_{\mathsf{R}}(\varphi^{m,n}(\vartheta_s^m)) = \left|\mathsf{AF}(\varphi^{m,n}(\vartheta_s^m))\right|^2 \tag{2}$$

where

$$\varphi^{m,n}(\vartheta_s^m) = \arcsin\left(\sin(\varphi_{\mathsf{AZ}}^{m,n} - \vartheta_s^m)\cos(\varphi_{\mathsf{EL}}^{m,n})\right) \tag{3}$$

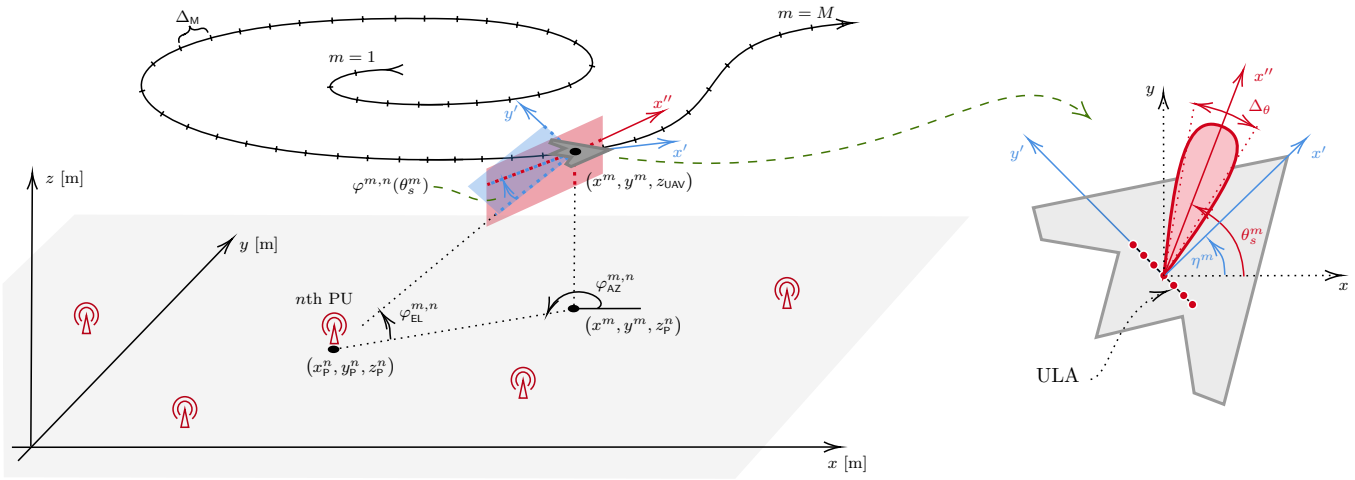

Fig. 1. The system model and the frames of reference. The UAV collects measurements along the pre-planned trajectory over ground-based PUs to be located (red transmitters). The azimuth plane of the UAV is illustrated on the right where the steering antenna beam is depicted in red (only the mainlobe).

with $\varphi_{\mathsf{AZ}}^{m,n}$ and $\varphi_{\mathsf{EL}}^{m,n}$ the azimuth and elevation angles of the DoA, respectively given by (see Fig. 1)

$$\varphi_{\mathsf{AZ}}^{m,n} = \arctan\Big(\big(y_{\mathsf{P}}^n - y^m\big)/\big(x_{\mathsf{P}}^n - x^m\big)\Big) \tag{4}$$

$$\varphi_{\mathsf{EL}}^{m,n} = \arctan\left(\frac{z_{\mathsf{UAV}} - z_{\mathsf{P}}^n}{\sqrt{(x_{\mathsf{P}}^n - x^m)^2 + (y_{\mathsf{P}}^n - y^m)^2}}\right) \tag{5}$$

and $\arctan(\cdot)$ the four quadrant inverse tangent. Note that since the AF in (1) achieves the maximum value, U, when $\varphi = 0$, the array gain is maximum when $\varphi^{m,n}(\vartheta_s^m) = \vartheta_s^m$. Moreover, the PU's height is unknown, but significantly smaller than z_{UAV}.

We denote with $P_s^{m,n}$ the power received from the nth PU, when the UAV is at $\boldsymbol{\ell}^m$ and the ULA beam is steered towards ϑ_s^m, as

$$P_s^{m,n}(\varphi^{m,n}(\vartheta_s^m)) = \frac{P_{\mathsf{T}}^n G_{\mathsf{T}} G_{\mathsf{R}}(\varphi^{m,n}(\vartheta_s^m))}{\mathsf{PL}\big(\|\boldsymbol{\ell}_{\mathsf{P}}^n - \boldsymbol{\ell}^m\|_2\big)} \tag{6}$$

where G_{T} is the transmit antenna gain considered isotropic, and $\mathsf{PL}(d)$ is the path-loss at distance d. In the presence of N PUs, the RSS when the array pattern points towards ϑ_s^m is therefore

$$P_s^m = \sum_{n=1}^{N} P_s^{m,n} X_m^n + P_{\mathsf{N}} \tag{7}$$

where P_{N} is the receiver noise power (at the RSS sensor onboard the UAV), and X_m^n represents a discrete-time two-state Markov chain which characterize the activity pattern of the PUs. In particular, $X_m^n = 0$ when the nth PU is idle, $X_m^n = 1$ when it is active, and the transition matrix between the two states is

$$\mathbf{T} = \begin{bmatrix} 1 - p_{01} & p_{01} \\ p_{10} & 1 - p_{10} \end{bmatrix} \tag{8}$$

where $p_{01} = \mathbb{P}\{X_{m+1}^n = 1 \,|X_m^n = 0\}$, and $p_{10} = \mathbb{P}\{X_{m+1}^n = 0 \,|X_m^n = 1\}$. Accordingly, the vector of received power at mth measurement is $\mathbf{p}^m = [P_1^m, P_2^m, \ldots, P_S^m]$.

Note that the proposed algorithm does not depend on the channel model, so the path-loss $\mathsf{PL}(d)$ in (6) can be represented by any propagation model suitable for the environment. Examples are the power-law path-loss with log-normal shadowing, the directional channel model [34], and the air-to-ground channel model [35], [36]. For the trajectory, because of the map formation mechanisms described in the next section, we recommend a UAV path circumscribing the area, e.g., a large circular-like trajectory. In Section V, we present the channel model, trajectory, and other system parameters, as a recommendation for the reader.

The proposed UAV-aided multiple PU localization technique can be divided into two phases described in the following two sections: 1) score map construction, and 2) detection and localization of the PUs.

III. Mapping via UAV

Let us divide the monitoring area into $L \times L$ grid points, $\boldsymbol{\ell}_{i,j} = [x_i, y_j]$, $i, j = 1, \ldots, L$, with spacing $\Delta_{\mathsf{G}} = \mathscr{L}/(L-1)$. The M measurements are taken by the UAV along its pre-planned trajectory with steps of length Δ_{M}.

In the following, we construct a score map based on the steering direction and the RSS, that exhibit peaks where the PUs are present. The proposed approach is detailed in Algorithm 1. Here is the summary of the main steps to build the score map:

1) Collect the measurements from onboard UAV sensors, $\mathcal{M}^m = \{\boldsymbol{\ell}^m, \eta^m, \mathbf{p}^m\}$, i.e., UAV position, heading direction, and RSSs. The received powers are gathered by steering step-by-step the ULA at angles $\vartheta_s^m = \vartheta_1^m + \Delta_\vartheta(s-1)$, $s = 1, \ldots, S$.
2) The azimuth angle of the grid point $\boldsymbol{\ell}_{i,j}$ seen at the mth measurement position is calculated as
$$\phi_{\mathsf{AZ}}^{m,i,j} = \arctan\left(\frac{y_j - y^m}{x_i - x^m}\right). \tag{9}$$
3) Assign the score value to the grid point. At the mth measurement, the grid point at position $\boldsymbol{\ell}_{i,j}$ has a score
$$s_{i,j}^m = \sum_{s=1}^{S} P_s^m G_{\mathsf{R}}\big(\beta_{i,j}^m(\vartheta_s^m)\big) \tag{10}$$

Algorithm 1 UAV Mapping

```
Get {M^m}_{m=1}^M, Δ_ϑ, and L
for m = 1 : M do
    ϑ_s^m ← η^m + (s − 1)Δ_ϑ, s = 1, ..., S
    for all ℓ_{i,j} with i = 1, ..., L, j = 1, ..., L do
        φ_{i,j}^m ← arctan((y_j − y^n)/(x_i − x^m))
        for s with s = 1, ..., S do
            s_{i,j}^m ← Σ_{s=1}^S P_s^m G_R(β_{i,j}^m(ϑ_s^m))
        end for
    end for
    s_{i,j} ← Σ_{m=1}^M s_{i,j}^m
end for
```

where $\beta_{i,j}^m(\vartheta_s^m)$ is the broadside angle of the grid point (the elevation angle is set to 0°, so it also equals to the azimuth angle) seen from the measurement position, given by

$$\beta_{i,j}^m(\vartheta_s^m) = \phi_{\mathsf{AZ}}^{m,i,j} - \vartheta_s^m. \tag{11}$$

The equation (10) is a weighted sum of power received at different directions, s, where the array gain represents the weights. This way, every point in the grid has a weight proportional to the actual radiation diagram. Hence, for example, all grid points seen by the main lobe have large weights.

4) Sum up the score as per measurement at each grid point

$$s_{i,j} = \sum_{m=1}^{M} s_{i,j}^m. \tag{12}$$

The score map is indicated by the $L \times L$ matrix $\mathcal{S} = \{s_{i,j}\}$.

In Fig. 2, an example of map formation during a UAV pass is shown as a series of cumulative maps at measurement positions $t = \{1, 10, 30, 50, 70, 100\}$, with $M = 100$, defined as

$$\mathcal{S}^{1\to t} = \sum_{m=1}^{t} \mathcal{S}^m \tag{13}$$

where $\mathcal{S}^m = \{s_{i,j}^m\}$ and $\mathcal{S}^{1\to M} = \mathcal{S}$. As can be seen, with just one measurement (Fig. 2a), the score map exhibits numerous local maxima and minima and an ambiguous profile. However, as the UAV moves along the trajectory, the score map progressively assumes a shape with few, well-defined peaks around the true PU locations, revealing the presence of multiple transmitters and their positions. Note that, as per the system model, the map formation does not require any prior information about the number, position, activity pattern, and transmit power of the PUs.

IV. Detection and Localization

We propose two methods for the second phase: a) KCWC technique, which requires two scenario dependent parameters with a relatively low computational cost; and b) GMMF approach, which is non-parametric, but more computational demanding than KCWC.

A. K-means Clustering and Weighted Centroid Method

To process the score map, we propose the KCWC method to estimate the number and positions of PUs with no extra prerequisites. The algorithm requires only one parameter, the threshold α (dimensionless). KCWC is detailed in Algorithm 2, and here summarized:

1) Set a threshold on the score map to find a coarse estimate of the regions containing potential PUs

$$\mathcal{S}_{\mathsf{TH}} = \mathcal{S}_{\mathsf{MIN}} + \alpha(\mathcal{S}_{\mathsf{MAX}} - \mathcal{S}_{\mathsf{MIN}}) \tag{14}$$

where $\mathcal{S}_{\mathsf{MAX}} = \max_{i,j}\{s_{i,j}\}$, $\mathcal{S}_{\mathsf{MIN}} = \min_{i,j}\{s_{i,j}\}$, and $\alpha \in [0, 1]$.

2) Generate a new sub-map $\bar{\mathcal{S}}$ by removing the grid points with score values below the threshold. When α is large (i.e., close to 1), only a few points $s_{i,j}$ of the map are selected, resulting in low false alarms but also in misdetection of PUs. On the contrary, if α is small the sub-map may lead to many false alarms but high detection rates. Group the grid points in the sub-map $\bar{\mathcal{S}}$ into clusters by k-means clustering. The cluster number can be estimated by the GAP criterion working for scenarios containing only one or multiple clusters [37].[1] The cluster label per grid point is denoted as $c_{i,j}$, and the kth cluster is identified by the set of grid points $\mathcal{C}_k = \{(i, j) : c_{i,j} = k\}$.

3) An estimate of the number of PUs is given by the optimal cluster number, i.e.,

$$\widehat{N} = \max_{i,j}\{c_{i,j}\}. \tag{15}$$

4) The estimates of PU positions are calculated by WCL among all the grid points within the cluster [14], [19]. The estimate of the kth PU position is then given by

$$\widehat{\boldsymbol{\ell}}_{\mathsf{P}}^k = \left[\widehat{x}_{\mathsf{P}}^k, \widehat{y}_{\mathsf{P}}^k\right] = \left[\frac{\sum\limits_{(i,j)\in\mathcal{C}_k} \omega_{i,j} x_i}{\sum\limits_{(i,j)\in\mathcal{C}_k} \omega_{i,j}}, \frac{\sum\limits_{(i,j)\in\mathcal{C}_k} \omega_{i,j} y_j}{\sum\limits_{(i,j)\in\mathcal{C}_k} \omega_{i,j}}\right] \tag{16}$$

where the weighting coefficients

$$\omega_{i,j} = \frac{s_{i,j} - \mathcal{S}_{\mathsf{MIN}}}{\mathcal{S}_{\mathsf{MAX}} - \mathcal{S}_{\mathsf{MIN}}} \tag{17}$$

are based on the score map. More specifically, WCL computes a weighted average, the centroid, over the grid points within the cluster, where the weights are proportional to the score map.

B. Gaussian Mixture Model Fitting Method

This technique offers an alternative approach to estimate the number of PUs and their location without requiring any predefined parameter. We first evaluate the number of PUs by principal component analysis (PCA) applied to score maps generated at one fixed measurement position, for example, the first measurement. Note that PCA requires that PUs transmissions are non-continuous since the samples collected must contain a sufficiently large number of transitions (8).

[1] In this work, we used the GAP criterion clustering evaluation object offered by *evalclusters* function in Matlab.

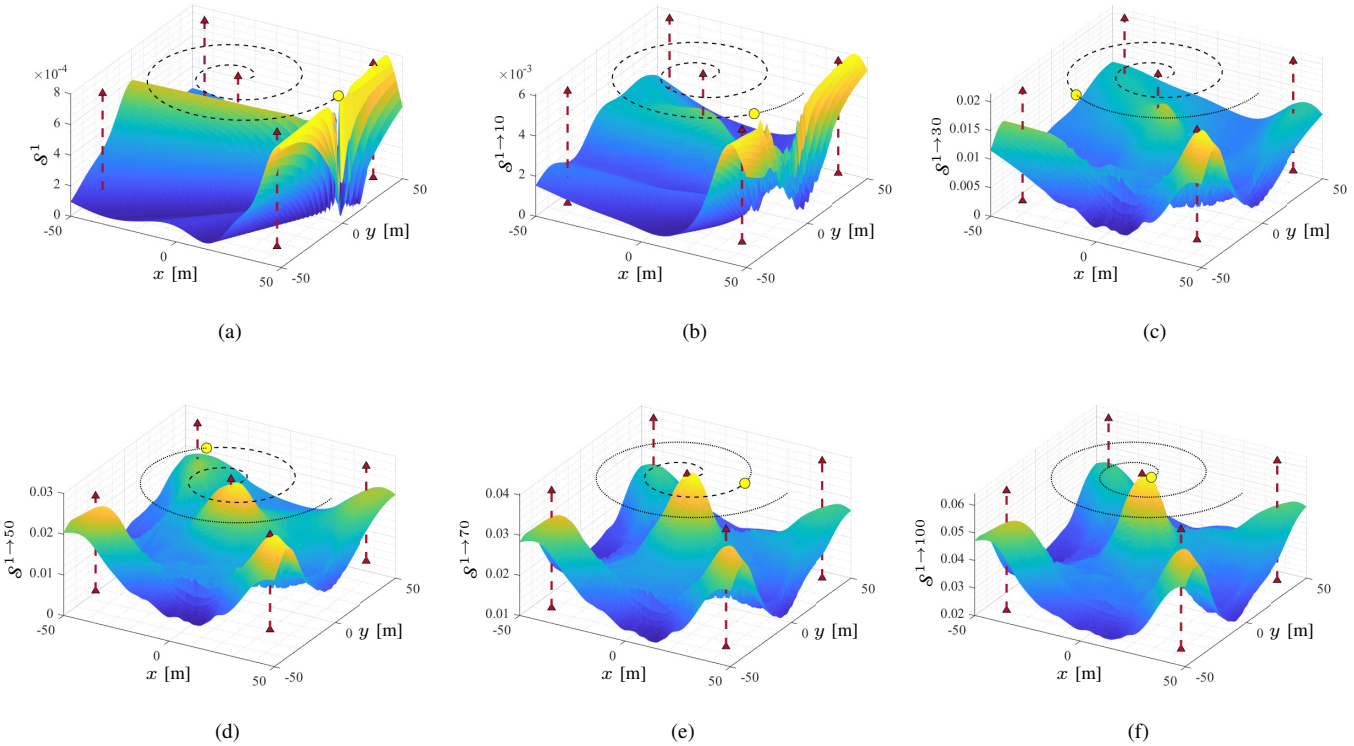

Fig. 2. An example of map formation process. The red triangles are the true PU positions and their 3-D projections along the z-axis. The black spiral is the UAV trajectory, along which dotted/dashed line illustrates 'already covered'/'to be covered' trajectory by the UAV, and the yellow circle depicts the current UAV position. The surface plots present the cumulative score map from the first measurement to the current position, $t = 1, 10, 30, 50, 70$, and 100 respectively from (a) to (f).

Algorithm 2 Detection and Localization - KCWC

Get $\mathcal{S}$, α
$\mathcal{S}_{\mathsf{MAX}} \leftarrow \max_{i,j}\{s_{i,j}\}$, $\mathcal{S}_{\mathsf{MIN}} \leftarrow \min_{i,j}\{s_{i,j}\}$
$\mathcal{S}_{\mathsf{TH}} = \mathcal{S}_{\mathsf{MIN}} + \alpha(\mathcal{S}_{\mathsf{MAX}} - \mathcal{S}_{\mathsf{MIN}})$
for all $s_{i,j}$ **do**
  if $s_{i,j} \geq \mathcal{S}_{\mathsf{TH}}$ **then**
    $\bar{s}_{i,j} \leftarrow s_{i,j}$
  else
    $\bar{s}_{i,j} \leftarrow$ null
  end if
end for
$c_{i,j} = \text{cluster}\{\bar{s}_{i,j}\}$
$\widehat{N} \leftarrow \max_{i,j}\{c_{i,j}\}$
for all $c_{i,j} = 1, \ldots, \widehat{N}$ **do**
  $\widehat{\boldsymbol{\ell}}_{\mathsf{P}}^{k} \leftarrow \left[\frac{\sum_{(i,j)\in c_k} \omega_{i,j} x_i}{\sum_{(i,j)\in c_k} \omega_{i,j}}, \frac{\sum_{(i,j)\in c_k} \omega_{i,j} y_j}{\sum_{(i,j)\in c_k} \omega_{i,j}}\right]$
end for

Then, a mixture of bivariate Gaussian functions is used to fit the score map defined in Section III via a Monte Carlo method. The approach is blind, hence powerful, at the cost of computational complexity. A detailed description is provided in Algorithm 3 and a summary is presented in the following:

1) Collect R score maps by steering the ULA beam by 2π and repeating for R times while the UAV is hovering at $\boldsymbol{\ell}^m$ with fixed heading direction η^m. Each score map is calculated according to (10) and denoted with $\mathcal{S}^{m,r}$, with $r = 1, \ldots, R$. Staking up the R score maps, the $L \times L \times R$ tensor $\mathcal{T}^m = \{s^m_{i,j,r}\}$ is obtained.
2) Reshape the tensor $\mathcal{T}^m$ to a $R \times L^2$ matrix by applying standard linear algebra tools. It is convenient to unfold it along the row and stack the transformed mode-2 fiber as the rth row of the $R \times L^2$ matrix $\mathcal{G} = \{g_{p,q}\}$ [38] as

$$g_{p,q} = s^m_{(q-1)/g+1,(q-1) \bmod g+1,p} \tag{18}$$

where a/b returns the quotient and $a \bmod b$ returns the remainder of the Euclidean division of a by b.
3) Perform singular value decomposition of the matrix $\mathcal{G}$, and denote with σ_k, $k = 1, \ldots, R$, the corresponding singular values.
4) An estimate of the number of PUs, $\widehat{N}$, is given by the number of singular values that are greater than the average [39], i.e.,

$$\widehat{N} = \sum_{k=1}^{R} \mathbb{1}_{\{\sigma_k > \bar{\sigma}\}} \tag{19}$$

with

$$\bar{\sigma} = \frac{1}{R} \sum_{k=1}^{R} \sigma_k \tag{20}$$

where $\mathbb{1}_{\{\mathcal{A}\}}$ is the indicator function, i.e., equal to one when $\mathcal{A}$ is true and zero otherwise.

Algorithm 3 Detection and Localization - GMMF

Get $\mathcal{S}$, ρ_{MAX}, ρ_{MIN}, and R
$\mathcal{S}^m \leftarrow \{s^m_{i,j,r}\}$
$g_{p,q} \leftarrow s^m_{(q-1)/g+1,(q-1) \bmod g+1,p}$
$\mathcal{G} \leftarrow \{g_{p,q}\}$
$\sigma_k \leftarrow \mathrm{svd}\{\mathcal{G}\}$, $k = 1, \ldots, R$
$\widehat{N} = \sum_{k=1}^{R} \mathbb{1}_{\{\sigma_k > \bar{\sigma}\}}$
$\mathcal{S}_{\mathsf{MAX}} \leftarrow \max_{i,j}\{s_{i,j}\}$, $\mathcal{S}_{\mathsf{MIN}} \leftarrow \min_{i,j}\{s_{i,j}\}$
$\rho_{i,j} = \mathrm{round}\left(\rho_{\mathsf{MIN}} + \frac{(\rho_{\mathsf{MAX}} - \rho_{\mathsf{MIN}})(s_{i,j} - \mathcal{S}_{\mathsf{MIN}})}{\mathcal{S}_{\mathsf{MAX}} - \mathcal{S}_{\mathsf{MIN}}}\right)$
Get $\mathscr{P}$ from histogram $\rho_{i,j}$
$\{\pi_n, \boldsymbol{\mu}_n, \boldsymbol{\Sigma}_n\} \leftarrow \mathrm{gmmf}\{\mathscr{P}\}$ given mixture size $\widehat{N}$
for $n = 1, \ldots, \widehat{N}$ **do**
  $\widehat{\boldsymbol{\ell}}^n_{\mathrm{p}} \leftarrow \boldsymbol{\mu}_n$
end for

5) In order to fit Gaussian mixture model to the score map, transform the score map $\mathcal{S}$ (12) into a particle map $\mathscr{P}$ following a Monte Carlo approach. Firstly, each score $s_{i,j}$ is scaled into $\rho_{i,j}$ between ρ_{MIN} and ρ_{MAX}

$$\rho_{i,j} = \mathrm{round}\left(\rho_{\mathsf{MIN}} + \frac{(\rho_{\mathsf{MAX}} - \rho_{\mathsf{MIN}})(s_{i,j} - \mathcal{S}_{\mathsf{MIN}})}{\mathcal{S}_{\mathsf{MAX}} - \mathcal{S}_{\mathsf{MIN}}}\right). \tag{21}$$

Then, repeat the position of the grid point $\boldsymbol{\ell}_{i,j}$ for $\rho_{i,j}$ times to generate the matrix of particles $\mathscr{P}$ of size $2 \times N_{\mathsf{P}}$, where $N_{\mathsf{P}} = \sum_{i,j} \rho_{i,j}$ and its two rows represent the x and y axis of the grid point. Thus the outline of the 2D histogram of $\mathscr{P}$ is similar to the shape of $\mathcal{S}$.

6) Apply standard GMMF to the particles $\mathscr{P}$, with the number of bivariate Gaussian component of the mixture equal to (19). In particular, GMMF aims at finding the best mixture of bivariate Gaussian kernels that fits the histogram $\rho_{i,j}$, i.e.,

$$\bar{\rho}_{i,j} = \sum_{n=1}^{\widehat{N}} \pi_n \mathcal{N}\big(\boldsymbol{\ell}_{i,j}; \boldsymbol{\mu}_n, \boldsymbol{\Sigma}_n\big) \tag{22}$$

where $\pi_n > 0$ are the weights associated to the mixture, while

$$\mathcal{N}(\boldsymbol{\ell}; \boldsymbol{\mu}, \boldsymbol{\Sigma}) = \frac{\exp\left(-\frac{1}{2}(\boldsymbol{\ell} - \boldsymbol{\mu})^{\mathsf{T}} \boldsymbol{\Sigma}^{-1} (\boldsymbol{\ell} - \boldsymbol{\mu})\right)}{2\pi\sqrt{\det(\boldsymbol{\Sigma})}} \tag{23}$$

with $\boldsymbol{\mu}_n$ the expected value, and $\boldsymbol{\Sigma}_n$ the 2×2 covariance matrix of the nth component, respectively. Such a mixture fitting problem is solved by the expectation-maximization (EM) and can be found as a routine in many statistical packages [40].[2]

7) The estimates of the PU locations are thus given by the mean vectors of the Gaussian components estimated by GMMF, i.e.,

$$\widehat{\boldsymbol{\ell}}^n_{\mathrm{p}} = \boldsymbol{\mu}_n \qquad n = 1, \ldots, \widehat{N}. \tag{24}$$

[2]For example, in this work, we used the *fitgmdist* function available in Matlab.

V. Case Study

This section introduces the simulation settings, including the channel model, the UAV trajectory, and the parameters used in the algorithms.

A. Channel Model

We adopt the A2G channel model proposed for an airborne scenario [35]. The path-loss under the A2G channel can be defined as the summation of excessive path-loss component and the free space path-loss, $\mathsf{PL}(d) = \varepsilon + \mathsf{FSPL}(d)$, when expressed in decibel. The free space path-loss $\mathsf{FSPL}(d)$ can be calculated by the Friis transmission equation. The term, ε, follows a normal distribution with mean, μ_ξ, and standard deviation, $\sigma_\xi(\varphi_{\mathsf{EL}})$, where ξ is the group number, 1 for LoS, or 2 for none-line-of-sight (NLoS). The mean, μ_ξ, is a constant, independent from the elevation angle. The standard deviation can be described by $\sigma_\xi(\varphi_{\mathsf{EL}}) = a_\xi \exp(-b_\xi \varphi_{\mathsf{EL}})$, where a_ξ and b_ξ are frequency and environment-dependent parameters, while φ_{EL} is the elevation angle in degrees. The occurrence probability of each group can be defined as $p_{\varphi_{\mathsf{EL}}}(1) = \mu \cdot (\varphi_{\mathsf{EL}} - \varphi_{\mathsf{EL}_0})^\nu$ and $p_{\varphi_{\mathsf{EL}}}(2) = 1 - p_{\varphi_{\mathsf{EL}}}(1)$, where φ_{EL_0} is selected as 15° corresponding to the minimum elevation angle supported by the model. In our case, we adopt the parameter values recommended for the urban scenario at $f_{\mathsf{C}} = 2\,\mathrm{GHz}$: $\mu_1 = 1.0$, $\mu_2 = 20$, $a_1 = 10.39$, $b_1 = 0.05$, $a_2 = 29.6$, $b_2 = 0.03$, $\mu = 0.6$, and $\nu = 0.11$. Parameters for other scenarios and frequencies can be found in Table II of [35].

B. Trajectory

The UAV flies over the area following an Archimedean spiral expressed by the equation, $\imath = a + \mathcal{b}\varphi$, in the polar coordinate system $(\imath, \varphi)$, where a and $\mathcal{b}$ control the turns and the distance between each turn, respectively. Assuming the inner end of the spiral is fixed at $[x_0, y_0]$, $a = x_0$, and $\mathcal{b} = \frac{g}{2\pi}$, where g is the spiral growth per turn. The total length of the spiral is

$$\mathscr{L}_{\mathsf{TR}} = \int_{\pi}^{2t\pi} \sqrt{(a + \mathcal{b}\varphi)^2 + \mathcal{b}^2} d\varphi \tag{25}$$

where t is the number of turns of the spiral. Then, the spacing of the measurements along the spiral is $\Delta_{\mathsf{M}} = \mathscr{L}_{\mathsf{TR}}/M \approx \imath \sin \Delta_\varphi$, where Δ_φ is the corresponding angular increment and where the approximation becomes better as Δ_φ gets smaller. In this case, it is easy to compute iteratively the angular increment that leads to equally spaced measurement by $\Delta^{(m)}_\varphi \approx \Delta^{(m-1)}_\varphi + \arcsin(\Delta_{\mathsf{M}}/\imath^{(m)})$. Note that the heading direction of the UAV η^m is tangent to the spiral.

C. System Overview

As shown in Fig. 1, we consider $N = 5$ PUs located at coordinates $\boldsymbol{\ell}^1_{\mathsf{P}} = [42, 40, 0]\,\mathrm{m}$, $\boldsymbol{\ell}^2_{\mathsf{P}} = [-39, 41, 0]\,\mathrm{m}$, $\boldsymbol{\ell}^3_{\mathsf{P}} = [-40, -41, 0]\,\mathrm{m}$, $\boldsymbol{\ell}^4_{\mathsf{P}} = [-41, -38, 0]\,\mathrm{m}$, $\boldsymbol{\ell}^5_{\mathsf{P}} = [0, 1, 0]\,\mathrm{m}$, within a square area of side length $\mathscr{L} = 100\,\mathrm{m}$ and grid spacing $\Delta_{\mathsf{G}} = 1\,\mathrm{m}$. The PUs transmit at frequency $f_{\mathsf{C}} = 2\,\mathrm{GHz}$ with power $P^n_{\mathsf{T}} = 0\,\mathrm{dBW}$, antenna gain $G_{\mathsf{T}} = 1$ and activity pattern defined by $p_{01} = 0.8$ and $p_{10} = 0.3$. The UAV cruises

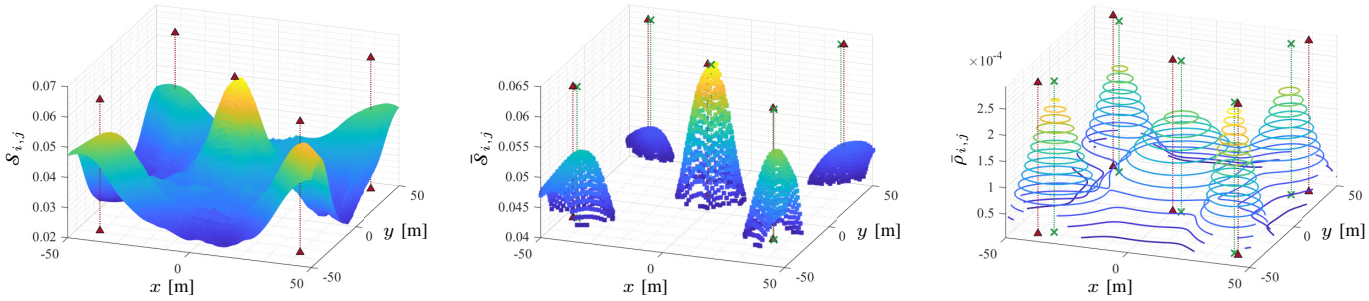

(a) (b) (c)

Fig. 3. (a) The score map with one realization of the channel. (b) The clustering and the results of KCWC method for $\alpha = 0.5$. (c) The fitting surface and results obtained by the GMMF method for $\rho_{\mathsf{MAX}} = 1000$, $\rho_{\mathsf{MIN}} = 0$, and $R = 100$. In all figures, the red triangles depict the true positions of the PUs, while in (b) and (c), the green crosses indicate the location estimates.

over the area at a height $z_{\mathsf{UAV}} = 50\,\mathrm{m}$ with a trajectory starting at $[5, 0, 50]$ m, with $t = 2$ turns, and spiral growth $g = 20\,\mathrm{m}$ (see Fig. 2). The number of measurement points along the trajectory is $M = 100$ with a spacing $\Delta_{\mathsf{M}} = 3.19\,\mathrm{m}$. The beamwidth of the ULA is $\Delta_\vartheta = 15^\circ$ which corresponds to $S = 24$ steering steps.[3] The receiver noise power of the RSS sensor on-board the UAV is $P_{\mathsf{N}} = -97.97\,\mathrm{dBm}$.

Following Algorithm 1, the score map of this scenario is created, and an example is shown in Fig. 3a. Intuitively, the five peaks illustrated by the score map indicate the positions of the PUs. The KCWC algorithm is then applied to the score map to estimate the number of PUs and their locations. Fig. 3b shows an example of the results from KCWC given $\alpha = 0.5$. The solution obtained by GMMF is depicted in Fig. 3c by contour plots of the map fitting for $\rho_{\mathsf{MAX}} = 1000$, $\rho_{\mathsf{MIN}} = 0$, and $R = 100$.

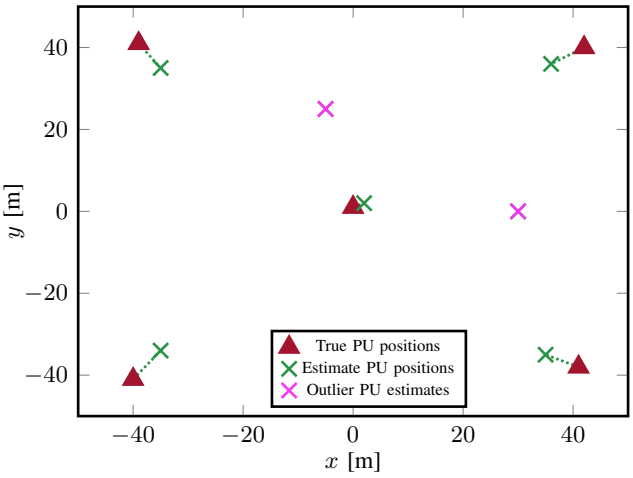

Fig. 4. An example of optimal subpattern assignment with $N = 5$ PUs and $\widehat{N} = 7$ estimated sources. Each true position of PU is paired with the closest estimate. The two remaining estimates are considered outliers.

VI. Performance Evaluation

This section evaluates the performance of the proposed localization algorithms by Monte Carlo simulations with 10^3 runs to account for different channel realizations and PUs' activity patterns.

The performance is evaluated in terms of OSPA metric [32] under different scenarios. The OSPA metric is a mis-distance indicator, which summarizes in a unique measure the estimation accuracy in both the number and location of the PUs. More precisely, given the true positions of N PUs, $\boldsymbol{\mathcal{L}} = \{\boldsymbol{\ell}_{\mathsf{P}}^1, \ldots, \boldsymbol{\ell}_{\mathsf{P}}^N\}$, and the $\widehat{N}$ estimates, $\widehat{\boldsymbol{\mathcal{L}}} = \{\widehat{\boldsymbol{\ell}}_{\mathsf{P}}^1, \ldots, \widehat{\boldsymbol{\ell}}_{\mathsf{P}}^{\widehat{N}}\}$, the distance between any pair of actual and estimated position cutoff at $c > 0$ is defined as [32]

$$d^{(c)}\{\boldsymbol{\ell}_{\mathsf{P}}^n, \widehat{\boldsymbol{\ell}}_{\mathsf{P}}^{\hat{n}}\} = \min\left\{c, d\{\boldsymbol{\ell}_{\mathsf{P}}^n, \widehat{\boldsymbol{\ell}}_{\mathsf{P}}^{\hat{n}}\}\right\} \tag{26}$$

where $d\{\boldsymbol{\ell}_{\mathsf{P}}^n, \widehat{\boldsymbol{\ell}}_{\mathsf{P}}^{\hat{n}}\} = \|\boldsymbol{\ell}_{\mathsf{P}}^n - \widehat{\boldsymbol{\ell}}_{\mathsf{P}}^{\hat{n}}\|_2$ is the Euclidean distance between the estimate and the true position. Denote by Π_k the set of permutations on $\{1, \ldots k\}$ for any $k \in \mathbb{N}$, for $1 \le p < \infty$ and $c > 0$, the OSPA distance of order p cutoff at c is defined as [32]

$$\mathcal{D}_p^{(c)}(\boldsymbol{\mathcal{L}}, \widehat{\boldsymbol{\mathcal{L}}}) = \left(\frac{1}{\widehat{N}}\left(\min_{\zeta \in \Pi_{\widehat{N}}} \sum_{i=1}^{N} \left(d^{(c)}\{\boldsymbol{\ell}_{\mathsf{P}}^i, \widehat{\boldsymbol{\ell}}_{\mathsf{P}}^{\zeta(i)}\}\right)^p + (\widehat{N} - N)c^p\right)\right)^{1/p} \tag{27}$$

if $N \le \widehat{N}$, and $\mathcal{D}_p^{(c)}(\boldsymbol{\mathcal{L}}, \widehat{\boldsymbol{\mathcal{L}}}) = \mathcal{D}_p^{(c)}(\widehat{\boldsymbol{\mathcal{L}}}, \boldsymbol{\mathcal{L}})$ if $N > \widehat{N}$. Basically, the OSPA distance can be obtained by the following steps:

1) Find the subset of $\widehat{\boldsymbol{\mathcal{L}}}$ that has the shortest distance to $\boldsymbol{\mathcal{L}}$, corresponding to the optimal subset assignment, as shown in Fig. 4;
2) If a point $\widehat{\boldsymbol{\ell}}_{\mathsf{P}}^{\hat{n}} \in \widehat{\boldsymbol{\mathcal{L}}}$, is not paired with any point in $\boldsymbol{\mathcal{L}}$, let $d_{\hat{n}} = c$; otherwise, $d_{\hat{n}}$ is the minimum value between c and the distance between the two points in a pair;
3) The OSPA distance is given by $\mathcal{D}_p^{(c)}(\boldsymbol{\mathcal{L}}, \widehat{\boldsymbol{\mathcal{L}}}) = \left(\sum_{\hat{n}=1}^{\widehat{N}} d_{\hat{n}}^p / \widehat{N}\right)^{1/p}$.

In the numerical results, we adopt $p = 2$ as recommended by [32] and $c = 10\,\mathrm{m}$ based on the area size and the expected

[3]This beamwidth can be achieved by a ULA with $U = 10$ elements spaced by $\Delta_{\mathsf{U}} = 0.05\,\mathrm{m}$ operating at f_{C}.

PU density. To lighten the notation, in the following we denote with $\mathscr{D}$ the OSPA distance $\mathscr{D}_2^{(10)}(\boldsymbol{\mathcal{L}}, \widehat{\boldsymbol{\mathcal{L}}})$ expressed in meters.

In the following, we adopt the average OSPA metric (averaged over Monte Carlo realizations) to evaluate the performance of KCWC and GMMF methods and compare them with a benchmark named GA which relies on the assumption that PU signals can be perfectly separated [25]. This last approach can be considered a lower bound in terms of OSPA. Moreover, to gain insight into the problem, the impacts of the main system parameters such as the number of measurements, UAV position and heading direction uncertainty, random PU positions, as well as random transmit power, are assessed. Finally, the capability to resolve close PUs is investigated.

A. Impact of α

In the KCWC method, the threshold α determines which grid points are selected for the successive clustering. In this section, we investigate the impact of α as a hyperparameter on the localization performance of KCWC under three channel conditions: suburban, urban, and dense urban. The channel models are generated by the method introduced in Section V-A, and the parameters follow the corresponding groups in Table II of [35].

As shown in Fig. 5, the impacts of α under different channels share a similar trend. Specifically, as α increases from 0.2 to 0.7, the OSPA plot follows a U-shape. The maximum value exceeds $7\,\mathrm{m}$ at both ends of α, and the minimum reaches down to $2-3\,\mathrm{m}$ with $\alpha = 0.5$. The reason is that a small α tends to merge peaks because of insufficient gaps between clusters. On the contrary, a large α might filter out weak peaks before the clustering process, ending up in an underestimate of the number of PUs. In the following results, we consider $\alpha = 0.5$ as the optimal value. Note that although in principle the choice of α may depend on the scenario, the UAV trajectory, and the clustering mechanism, Fig. 5 shows that its value is not critical because of a rather flat behaviour near the minimum. The reason is that there is a tolerance for α, which stems from the ability to separate peaks within the score map. As demonstrated in Section VI-E, wherein the number and locations of PUs are random, the value $\alpha = 0.5$, ensures very good localization accuracy.

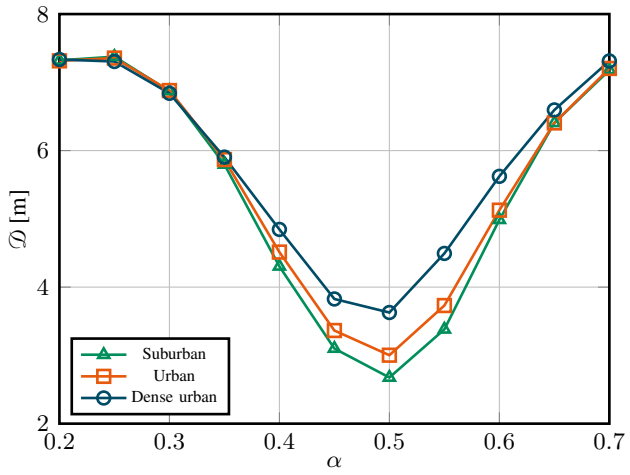

Fig. 5. The impact of α evaluated by OSPA distance in meters with respect to different propagation channel conditions.

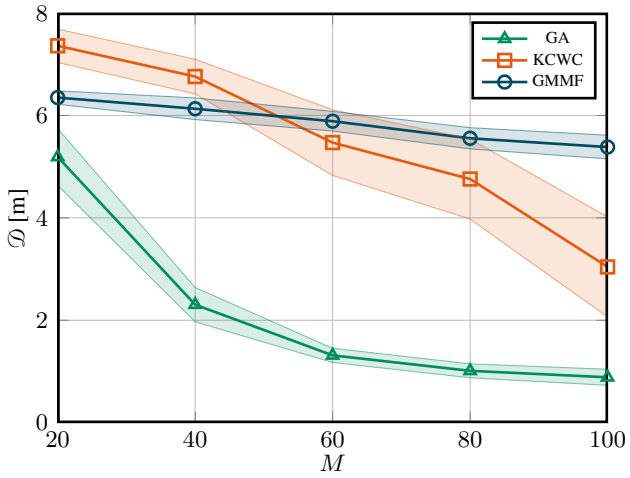

Fig. 6. The impact of the number of measurement M on the OSPA distance in meters. The shading amplitude is equal to the standard deviation of OSPA, while the thick line represents the average OSPA.

B. Impact of Number of Measurements

A relevant aspect investigated here is how the number of measurements affects the performance of the proposed algorithms. Keeping fixed the UAV start point at $[5, 0]\,\mathrm{m}$ and the step size $\Delta_{\mathsf{M}} = 3.18\,\mathrm{m}$, the increase in M from 20 to 100 leads to a longer trajectory and better coverage of the area. Fig. 6 depicts the OSPA distance as a function of M, for the three methods, the GA, and the proposed KCWC and GMMF approaches. Compared with the sharp dropping of GA, GMMF experiences a mild decrease from roughly $6.5\,\mathrm{m}$ to $5.5\,\mathrm{m}$. KCWC is more sensitive to M than GMMF, as its OSPA distance reduces by half when M increases. As expected, GA exhibits the lowest OSPA distance, because it takes advantage of the capability to distinguish the PUs. Besides the average, the standard deviation of OSPA is also relevant. Among the solutions provided, KCWC has the largest standard deviation ranging from $0.7\,\mathrm{m}$ to almost $2\,\mathrm{m}$, while GMMF exhibits a small standard deviation of around $0.4\,\mathrm{m}$. This confirms that in this scenario GMMF is more robust to channel fluctuations. In general, the proposed algorithms achieve remarkably good results even compared with baseline GA considering that they are entirely blind.

C. Impact of Measurement Uncertainty

In this section, we consider the impact of the UAV position error and the heading direction error due to the uncertainties in the positioning device (e.g., Global Positioning System (GPS)). The position error vector, $\mathbf{e}_{\mathsf{POS}} = [e_{\mathsf{X}}, e_{\mathsf{Y}}]$, has independent components, e_{X} and e_{Y}, following a normal distribution with zero mean and standard deviation σ_{POS} (in meters). In addition, the heading direction error follows a zero mean truncated normal distribution bounded by half of the beamwidth, $e_{\mathsf{DIR}} \in [-\Delta_\vartheta/2, \Delta_\vartheta/2]$ with standard deviation σ_{DIR} (in degrees). Thus measurements corrupted by the position

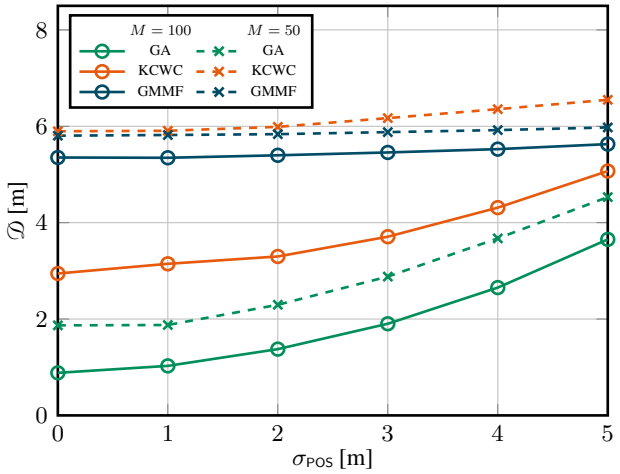

Fig. 7. The impact of the UAV position uncertainty on OSPA distance.

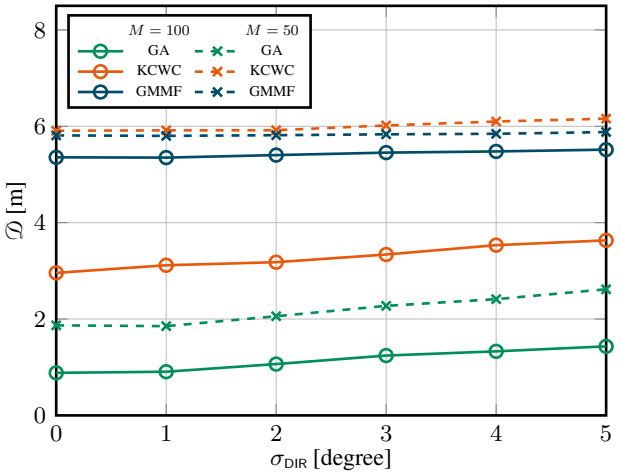

Fig. 8. The impact of the UAV heading direction uncertainty on OSPA distance.

error and heading direction error are $\mathcal{M}_{\text{POS}} = \{\boldsymbol{\ell} + \mathbf{e}_{\text{POS}}, \eta, \mathbf{p}\}$ and $\mathcal{M}_{\text{DIR}} = \{\boldsymbol{\ell}, \eta + e_{\text{DIR}}, \mathbf{p}\}$, respectively. Typically, a GPS receiver achieves horizontal accuracy of 3 m [41] and the heading angle accuracy is in the range 0.2 to 2 degree for small UAVs [42]. Thus, considering a scenario with urban canyons, in this section, we investigate σ_{POS} from 0 to 5 m, and σ_{DIR} from 0 to 5 degree.

Fig. 7 and Fig. 8 illustrate the impact of position error and heading direction error varying σ_{POS} and σ_{DIR} with $M = 50$ and 100. Both figures show an increasing trend for the three localization methods as the magnitude of the error increases, as expected. The benefit of a longer trajectory (larger M) is also evident. In line with previous results, GA performs the best, followed by KCWC and GMMF, although it appears more sensitive to position errors: the OSPA distance doubled when σ_{POS} increases from 0 to 5 m, while on the contrary GMMF deteriorates the least with severe errors. Moreover, it is interesting to note that for small M GMMF performs slightly better than KCWC. Regarding the OSPA standard deviation, KCWC exhibits the largest at around 2 m, while GMMF guarantees 0.3 m. To notice that for $M = 100$ while on average the error decreases the standard deviation is bigger than $M = 50$ and reaches 1.9 m. Again, considering that the proposed solutions are blind, their performance is very promising and robust to errors.

D. PUs Resolution Capability

In this section, we investigate the capability of the proposed methods to separate closely spaced PUs, i.e., the resolution. We simplify the scenario by considering the following two cases: 1) two PUs placed on the diagonal of the square area, and 2) five PUs on a circle centered at the origin of the area, with number of measurements $M = 50$ and 100. The performance is evaluated in terms of OSPA distance and the number of estimated PUs, both averaged over the Monte Carlo simulations. In the first case, the distance of the two PUs varies from $D_{\text{PU}} = 10$ to 30 m with steps of 2 m. As shown in Fig. 9, GMMF method can always separate the two PUs with both M. Although the OSPA distance of $M = 100$ outperforms that of $M = 50$, both of them remain around $\mathcal{D} = 8.5$ m. This is because the number of PUs is estimated correctly by PCA, but GMMF cannot localize the positions with high accuracy. On the contrary, KCWC method is more sensitive to the distance between the two PUs but achieves better performance for sufficiently spaced transmitters. For $M = 100$, the critical D_{PU} distance lies between 20 m and 24 m, where the PUs are spaced apart enough to be distinguished by KCWC (with $\alpha = 0.5$). Note that, as expected, the OSPA distance drops sharply when the number of the PUs is estimated correctly. However, the GAP criterion for optimal cluster number determination results in small overestimation when two PUs are more than 26 m apart. On the other hand, the KCWC performance for $M = 50$ shows a different trend from $M = 100$. The estimated number of PU increases mildly from 1 to 3 and the OSPA distance experiences little change. The mild increase of OSPA with the spacing is because the position estimate is achieved by WCL within one cluster (Step 5 of Section IV-A), which can be affected by the shape of the cluster and the weighting of the grid points within the cluster. The standard deviation of $\widehat{N}$ for GMMF is negligible, while the standard deviation of $\mathcal{D}$ is above 1 m when $M = 100$. For KCWC, the sharp drop of $\mathcal{D}$ at $D_{\text{PU}} = 20$ m to 24 m also experiences the largest standard deviation up to 3.5 m.

In the second case, five PUs are placed on a circle with equal spacing on the arc. The straight line distance between two neighbouring PUs increases from $D_{\text{PU}} = 10$ m to 50 m with increments of 5 m. Consequently, the radius of the circle increases from $R_{\text{PU}} = 8.50$ m to $R_{\text{PU}} = 42.53$ m with increments of 4.25 m. As shown in Fig. 10, similar to the two PU case, a greater M improves the performance of KCWC more than GMMF. GMMF method, with both M, achieves correct estimation of the number of PUs when $D_{\text{PU}} > 25$ m. Thus, the OSPA distance drops to roughly 6 m. However, the behavior of KCWC is more complicated. Despite the increase in M and D_{PU}, the estimated number of PU is not accurate because the layout of the PUs limits the performance of the GAP criterion. Correspondingly, for $M = 100$, the OSPA distance drops to 3 m, when $\widehat{N} = 5$ and $D_{\text{PU}} = 25$ m, but

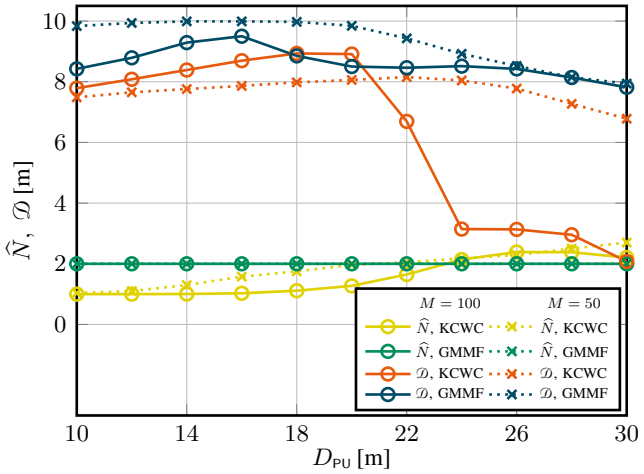

Fig. 9. The OSPA distance and the average number of estimated nodes, as a function of the distance between PUs, with $N = 2$, $M = 100$ and 50.

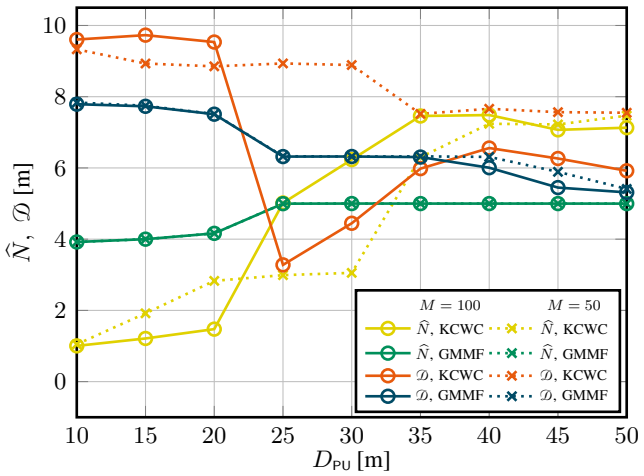

Fig. 10. The OSPA distance and the average number of estimated nodes, as a function of the distance between PUs, with $N = 5$, $M = 100$ and 50.

it increases to more than 6 m, when D_{PU} is larger and the number of PU is overestimated.

E. Random PUs Scenario

In the above discussions, we have presented the impact of various factors on the localization performance when two or five PUs are located at pre-selected positions rather evenly in the area of interest. In this section, we look into the scenarios wherein there is randomness in the number, the positions, and the transmit power of the PUs. Specifically, we assume that the number of PUs are uniformly drawn between 1 to 6, and their positions are also random in the area with a minimum distance of 20 m between each other. As for the transmit power, we consider two cases: i) transmit power identical for all the PUs an equal to $P_{\text{T}}^n = 0\,\text{dBW}$; ii) independent, identically distributed (i.i.d.) transmit powers with $P_{\text{T}} \in \{-10, 0\}\,\text{dBW}$ with equal probability. Monte Carlo realizations are now 2×10^3 while the other simulation parameters are unchanged.

Fig. 11 depicts the OSPA distance of these two random PU cases with the number of measurements increasing from $M =$

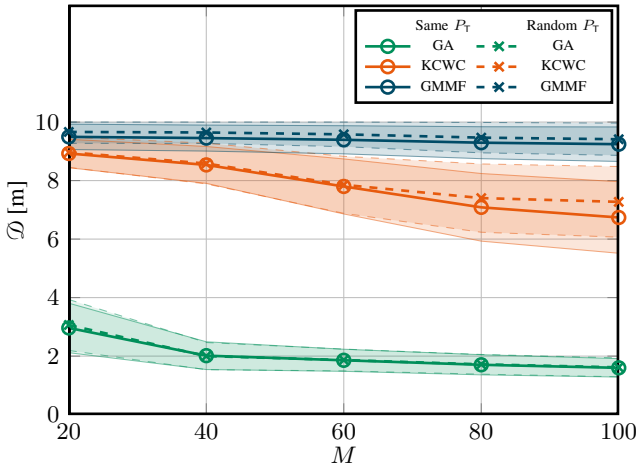

Fig. 11. The impact of the number of measurements M on the OSPA distance for scenarios with a random number of PUs, from 1 to 6, each one with a random position within the area. The shading amplitude is equal to the standard deviation of OSPA, while the thick lines with marks represent the average OSPA. The impact of random transmit power is also depicted.

20 to $M = 100$. As shown in the figure, the gap between non-blind (i.e.,GA) and blind (i.e., KCWC and GMMF) algorithm performance gets bigger due to the PU randomness. As can be expected, the variability of P_{T} hardly has any impact on the performance of GA, and the OSPA distance of random PUs is merely the same as the fixed five PU scenario. However, KCWC and GMMF experience a performance degradation. GMMF is the worst, stabling at roughly 9 m. The fixed P_{T} brings little improvement in the OSPA distance, neither does the increase in M. The first reason lies in the PCA capability that only about 20% of the realizations end up with correct PU number estimation. Among the correct cases, $N = 2$ and 3 take up to 88%, but $N = 5$ and 6 can hardly be estimated correctly. Fig. 10 also proves this result that at $D_{\text{PU}} = 20\,\text{m}$, $\widehat{N}$ is, on average, equal to 4. Another reason might be that random PU positions lead to the irregular shape of the peaks in the score map, which makes it challenging to fit Gaussian mixtures properly. On the other hand, the situation of KCWC is different. A large number of M improves the OSPA distance by 2 m, and the impact of random P_{T} is more pronounced with a bigger M. In summary, KCWC works better when PUs are not sufficiently distant, but GMMF can still be a good option if $N \leq 3$.

VII. Conclusion

In this work, we proposed the non-collaborative multiple PU localization by a UAV cruising over the monitored area. In particular, the solution requires only RSS measurement carried out by an antenna array with steering capabilities; hence it is blind and proved to be robust. The RSS measurement and steering angle are used to build up a score map. Then we designed two algorithms capable of performing PU number estimation and localization: k-means clustering and WCL, and Gaussian mixture model fitting. KCWC requires the proper choice of the threshold and has a relatively low computational cost. GMMF is parameter-free, but computationally expensive.

The performance evaluated by the OSPA distance demonstrated that both methods provide good localization accuracy, despite the lack of a priori knowledge of the signal structure and the simultaneous transmission of the PUs.

The proposed methodology is therefore promising but suggests further investigations, which may lead to different research directions. Firstly, the proposed algorithms achieve the best accuracy in the presence of LOS. While this situation is favored by air-to-ground UAV communications, it is still not completely clear how the approach performs in a dense urban scenario in NLOS conditions. Another interesting open problem is the possibility of using the approach when the area to be monitored is vast. In this scenario, we foresee a two-step localization: 1) build a score map based on a coarse grid, and perform rough targets counting and position estimation; 2) apply the localization algorithms to smaller areas (*divide et impera*) or redesign the UAV trajectory to fly-by the PUs.

REFERENCES

[1] M. Z. Win, F. Meyer, Z. Liu, W. Dai, S. Bartoletti, and A. Conti, "Efficient multisensor localization for the Internet of Things: Exploring a new class of scalable localization algorithms," *IEEE Signal Process. Mag.*, vol. 35, no. 5, pp. 153–167, Sep. 2018.

[2] A. Conti, S. Mazuelas, S. Bartoletti, W. C. Lindsey, and M. Z. Win, "Soft information for Localization-of-Things," *Proc. IEEE*, vol. 107, no. 11, pp. 2240–2264, Nov. 2019.

[3] A. Elzanaty, A. Giorgetti, and M. Chiani, "Limits on sparse data acquisition: RIC analysis of finite gaussian matrices," *IEEE Trans. Inf. Theory*, vol. 65, no. 3, pp. 1578–1588, Mar. 2019.

[4] R. Senanayake, P. J. Smith, P. A. Dmochowski, A. Giorgetti, and J. S. Evans, "Mixture detectors for improved spectrum sensing," *IEEE Trans. Wireless Commun.*, vol. 19, no. 6, pp. 4335–4348, Jun. 2020.

[5] H. Eltom, K. Sithamparanathan, Y. C. Liang, B. Moran, and R. J. Evans, "HMM based cooperative spectrum occupancy prediction using hard fusion," in *IEEE Int. Conf. on Comm. Workshops (ICC)*. IEEE, May 2016, pp. 669–675.

[6] E. Testi, E. Favarelli, L. Pucci, and A. Giorgetti, "Machine learning for wireless network topology inference," in *Proc. Int. Conf. on Signal Processing and Comm. Systems (ICSPCS)*, Gold Coast, Australia, Dec. 2019, pp. 1–7.

[7] R. Vaze and C. R. Murthy, "Multiple transmitter localization and whitespace identification using randomly deployed binary sensors," *IEEE Trans. on Cogn. Commun. Netw.*, vol. 2, no. 4, pp. 358–369, 2016.

[8] N. A. Jagadeesan and B. Krishnamachari, "A unifying bayesian optimization framework for radio frequency localization," *IEEE Trans. on Cogn. Commun. Netw.*, vol. 4, no. 1, pp. 135–145, 2018.

[9] J. Werner, J. Wang, A. Hakkarainen, D. Cabric, and M. Valkama, "Performance and cramer–rao bounds for DoA/RSS estimation and transmitter localization using sectorized antennas," *IEEE Trans. Veh. Technol.*, vol. 65, no. 5, pp. 3255–3270, May 2016.

[10] Y. Zeng, R. Zhang, and T. J. Lim, "Wireless communications with unmanned aerial vehicles: Opportunities and challenges," *IEEE Comm. Mag.*, vol. 54, no. 5, pp. 36–42, May 2016.

[11] C. Wang, J. Wang, Y. Shen, and X. Zhang, "Autonomous navigation of UAVs in large-scale complex environments: A deep reinforcement learning approach," *IEEE Trans. Veh. Technol.*, vol. 68, no. 3, pp. 2124–2136, 2019.

[12] A. Guerra, D. Dardari, and P. M. Djuric, "Dynamic radar networks of UAVs: A tutorial overview and tracking performance comparison with terrestrial radar networks," *IEEE Veh. Technol. Mag.*, vol. 15, no. 2, pp. 113–120, 2020.

[13] J. Blumenthal, R. Grossmann, F. Golatowski, and D. Timmermann, "Weighted centroid localization in zigbee-based sensor networks," in *Proc. IEEE Int. Symp. on Intelligent Sig. Proc. (WISP)*, vol. 5, Alcala de Henares, SPAIN, Oct. 2007, pp. 1–6.

[14] A. Mariani, K. Sithamparanathan, A. Giorgetti, and M. Chiani, "Cooperative weighted centroid localization for cognitive radio networks," in *Proc. IEEE Int. Symp. on Comm. and Inf. Tech., (ISCIT)*, Gold Coast, Australia, Oct. 2012, pp. 459–464.

[15] J. Wang, P. Urriza, Y. Han, and D. Cabric, "Weighted centroid localization algorithm: theoretical analysis and distributed implementation," *IEEE Trans. Wireless Commun.*, vol. 10, no. 10, pp. 3403–3413, Oct. 2011.

[16] S. Chaudhari and D. Cabric, "Cyclic weighted centroid algorithm for transmitter localization in the presence of interference," *IEEE Trans. on Cogn. Commun. Netw.*, vol. 2, no. 2, pp. 162–177, 2016.

[17] A. Giorgetti, K. Magowe, and K. Sithamparanathan, "Exact analysis of weighted centroid localization," in *Proc. European Sig. Pro. Conf. (EUSIPCO)*, vol. 24, Budapest, HUNGARY, Aug. 2016, pp. 743–747.

[18] K. Magowe, A. Giorgetti, K. Sithamparanathan, and X. Yu, "Statistical distribution of position error in weighted centroid localization," in *Proc. IEEE Int. Conf. on Commun.*, Paris, FRANCE, May 2017, pp. 1–5.

[19] K. Magowe, A. Giorgetti, K. Sithamparanathan, and X. Yu, "Accurate analysis of weighted centroid localization," *IEEE Trans. on Cogn. Commun. Netw.*, vol. 5, no. 1, pp. 153–164, Mar. 2019.

[20] E. Tohidi, J. Chen, and D. Gesbert, "Sensor selection for model-free source localization: where less is more," in *IEEE Int. Conf. on Acoustics, Speech and Signal Proc. (ICASSP)*, Barcelona, Spain, 2020, pp. 4831–4835.

[21] Q. Zhou, X. Li, and Y. Xu, "Mean shift based collaborative localization with dynamically clustering for wireless sensor networks," in *IEEE WRI Int. Conf. on Commun. and Mobile Computing*, vol. 2, Yunnan, China, Jan. 2009, pp. 66–70.

[22] K. Sithamparanathan and A. Giorgetti, *Cognitive Radio Techniques: Spectrum Sensing, Interference Mitigation and Localization*. Boston, USA: Artech House Publishers, Nov. 2012.

[23] W. Kim, J. Park, J. Yoo, H. J. Kim, and C. G. Park, "Target localization using ensemble support vector regression in wireless sensor networks," *IEEE Trans. Cybern.*, vol. 43, no. 4, pp. 1189—-1198, Nov. 2012.

[24] J. Chen, U. Yatnalli, and D. Gesbert, "Learning radio maps for UAV-aided wireless networks: A segmented regression approach," in *IEEE Int. Conf. on Communications (ICC)*, Paris, France, May 2017, pp. 1–6.

[25] Z. Li, K. Magowe, A. Giorgetti, and K. Sithamparanathan, "Blind localization of primary users with sectorial antennas," in *Proc. IEEE Int. Conf. on Comm. Work. (ICC Work.)*, Kansas City, MO, USA, May 2018, pp. 1–6.

[26] S. Sundberg and J. Garcia, "Sector fitting - a novel positioning algorithm for sectorized transmitters," in *IEEE Vehicular Tech. Conf. (VTC2020-Spring)*, Antwerp, Belgium, Belgium, May 2020, pp. 1–5.

[27] S. Choudhary and U. Mitra, "Analysis of target detection via matrix completion," in *IEEE Int. Conf. on Acoustics, Speech and Sig. Proc. (ICASSP)*, Brisbane, QLD, Australia, Apr. 2015, pp. 3771–3775.

[28] J. Chen and U. Mitra, "A tensor decomposition technique for source localization from multimodal data," in *IEEE Int. Conf. on Acoustics, Speech and Sig. Proc. (ICASSP)*, Calgary, AB, Canada, Apr. 2018, pp. 4074–4078.

[29] O. Esrafilian, R. Gangula, and D. Gesbert, "3D map-based trajectory design in UAV-aided wireless localization systems," *IEEE Internet of Things Journal*, pp. 1–11, 2020.

[30] J. Chen and U. Mitra, "Unimodality-constrained matrix factorization for non-parametric source localization," *IEEE Trans. Signal Process.*, vol. 67, no. 9, pp. 2371–2386, May 2019.

[31] J. Chen, "Exploiting two-dimensional symmetry and unimodality for model-free source localization in harsh environment," in *IEEE Int. Conf. on Acoustics, Speech and Signal Proc. (ICASSP)*, Barcelona, Spain, 2020, pp. 8294–8298.

[32] D. Schuhmacher, B. T. Vo, and B. N. Vo, "A consistent metric for performance evaluation of multi-object filters," *IEEE Trans. Signal Process.*, vol. 56, no. 8, pp. 3447–3457, Aug. 2008.

[33] S. J. Orfanidis, *Electromagnetic Waves and Antennas*, 1st ed. New Jersey, USA: Sophocles J. Orfanidis, 2016.

[34] Z. Li, K. Sithamparanathan, A. Giorgetti, A. Al-hourani, and K. Magowe, "Directional antenna channel modelling in urban area using ray tracing," *ITU Journal: ICT Discoveries*, vol. 2, no. 1, Nov. 2019.

[35] A. Al-Hourani, K. Sithamparanathan, and A. Jamalipour, "Modeling air-to-ground path loss for low altitude platforms in urban environments," in *Proc. IEEE Global Comm. Conf.*, Austin, TX, USA, Dec. 2014, pp. 2898–2904.

[36] N. H. Ranchagoda, K. Sithamparanathan, M. Ding, U. Thayasivam, and K. M. Gomez, "A building height-dependent gaussian mixture model to characterize air-to-ground wireless channels," in *Proc. IEEE Int. Conf. on Comm. Sys.*, Chengdu, China, Dec. 2018, pp. 173–179.

[37] R. Tibshirani, G. Walther, and T. Hastie, "Estimating the number of clusters in a data set via the gap statistic," *Journal of the Royal Statistical Society: Series B (Statistical Methodology)*, vol. 63, no. 2, pp. 411–423, 2001.

[38] A. Zare, A. Ozdemir, M. A. Iwen, and S. Aviyente, "Extension of PCA to higher order data structures: An introduction to tensors, tensor decompositions, and tensor PCA," *Proc. IEEE*, vol. 106, no. 8, pp. 1341–1358, July 2018.
[39] H. Abdi and L. J. Williams, "Principal component analysis," *Wiley Interdisciplinary Reviews: Comput. Stat.*, vol. 2, no. 4, pp. 433–459, Jul. 2010.
[40] C. M. Bishop, *Pattern Recognition and Machine Learning*. Springer Verlag, Aug. 2006.
[41] Department of Defense, United States of America, "Global positioning system standard positioning service performance standard," Available at https://www.gps.gov/technical/ps/2020-SPS-performance-standard.pdf (2021/03/31).
[42] R. Hirokawa and T. Ebinuma, "A low-cost tightly coupled GPS/INS for small UAVs augmented with multiple GPS antennas," *J. Inst. of Navig.*, vol. 56, no. 1, pp. 35–44, 2009.

Zhuyin Li received her B.Eng. degree in telecommunications engineering from Xiamen University, Fujian Province, China in 2011. She is currently a PhD candidate in electronics & telecommunications engineering, RMIT University, Melbourne, Victoria, Australia.

She won the scholarship of the department twice during her undergraduate study. From 2011 to 2013, she was a Product Management Engineer in the wireless network industry in Shenzhen, Guangdong, China. She worked as a short-term visiting research student in the Department of Electrical, Electronic, and Information Engineering of University of Bologna, Italy in 2018 and 2019 respectively. She is now on the RTP stipend scholarship funded by the Australia Government and the school-based stipend scholarship by the university. Her research interests include wireless channel modelling, directional channel propagation, blind localization and localization with directional antennas.

Andrea Giorgetti received the Dr. Ing. degree (summa cum laude) in electronic engineering and the Ph.D. degree in electronic engineering and computer science from the University of Bologna, Italy, in 1999 and 2003, respectively. From 2003 to 2005, he was a Researcher with the National Research Council, Italy. He joined the Department of Electrical, Electronic, and Information Engineering "Guglielmo Marconi," University of Bologna, as an Assistant Professor in 2006 and was promoted to Associate Professor in 2014. In spring 2006, he was with the Laboratory for Information and Decision Systems (LIDS), Massachusetts Institute of Technology (MIT), Cambridge, MA, USA. Since then, he has been a frequent visitor to the Wireless Information and Network Sciences Laboratory at MIT, where he presently holds the Research Affiliate appointment. His research interests include ultrawide bandwidth communication systems, active and passive localization, wireless sensor networks, and cognitive radio. He has co-authored the book Cognitive Radio Techniques: Spectrum Sensing, Interference Mitigation, and Localization (Artech House, 2012). He was the Technical Program Co-Chair of several symposia at the IEEE Int. Conf. on Commun. (ICC), and IEEE Global Commun. Conf. (Globecom). He has been an Editor for the IEEE COMMUNICATIONS LETTERS and the IEEE TRANSACTIONS ON WIRELESS COMMUNICATIONS. He has been elected Chair of the IEEE Communications Society's Radio Communications Technical Committee (2017-2018).

Professor Kandeepan Sithamparanathan is currently the Discipline Leader for Telecommunications & Photonics in the School of Engineering at the RMIT University. His areas of expertise include communication engineering, signal processing and networks applied in wireless, satellite and mobile systems. He has extensive experience in working with the industry for bringing research to practice as well as conducting fundamental research. Currently he works on several research projects such as; with the Defence Science Technology (DST) on intelligent spectrum management for a Defence-CRC project, with Bosch Australia for adopting 5G & IoT capabilities in automobile systems, and with several VIC based City Councils for experimenting and deploying IoT networks systems in the state of VIC-Australia. His current areas of interest are in 5G/6G wireless communications, satellite-aerial terrestrial communication systems, cognitive (satellite) radios, and IoT communications. He has authored a scholarly book on Cognitive Radio Techniques: Spectrum Sensing, Interference Mitigation and Localization, published by Artech House (New York) in 2012, and has published over 135 peer reviewed scientific journals and conference papers. Prof Sithamparanathan currently engages with the ITU as an academic member, was the Chair of IEEE Comsoc VIC chapter, was the Vice Chair of the IEEE Tech Committee on Cognitive Networks, and had received the RMIT Research Excellence Award in 2019 for his research work with the industry.